Available online at www.sciencedirect.com
ScienceDirect
Solar Energy xxx (2008) xxx–xxx
SOLAR ENERGY
www.elsevier.com/locate/solener

Solar sintering of alumina ceramics: Microstructural development

R. Román [a,*], I. Cañadas [b], J. Rodríguez [b], M.T. Hernández [a], M. González [a]

[a] EURATOM-CIEMAT Association, Avda. Complutense, 22, 28040 Madrid, Spain
[b] PSA-CIEMAT, P.O. Box 22, 04200 Tabernas, Almería, Spain

Received 21 June 2007; received in revised form 29 December 2007; accepted 1 April 2008

Communicated by: Associate Editor Robert Pitz-Paal

Abstract

Alumina powders were lab-synthesized and then sintered on a solar furnace (SF) in order to test the capability of these solar devices to produce dense ceramic bodies. The special configuration of the SF at PSA, Almeria (Spain), allowed to perform several experiments using high temperatures (up to 1780 °C), fast heating rates (50 and 100 °C min^{-1}) and different atmospheres (air, Ar and $95N_2$:$5H_2$). For comparison, similar alumina samples were sintered in an electric furnace (EF) using standard conditions (5 °C min^{-1} at 1600 °C during 240 min in air). An exhaustive microstructural characterization by scanning (SEM) and transmission (TEM) electron microscopies were performed on the sintered materials. Results for SF-samples showed a well-sintered alumina matrix of polyhedral grains even using shorter dwell times and higher heat-up rates than the conventional sintering. Obtained microstructures are in agreement with the presence of some impurities (mainly SiO_2, CaO, ZrO_2 and MgO) which are distributed at grain boundaries, triple points and matrix voids. For solar treatments, the variations of sintering parameters produced significant changes on matrix grain size, porosity and distribution of second phases. An important grain growth and density increase was observed after solar sintering on those tests performed at 1780 °C and under N_2:H_2 sintering atmosphere. The gathered data point out once more the convenience of SFs as sintering reactors to obtain ceramic materials with improved grain sizes.

Keywords: Alumina; Solar sintering; Microstructure

1. Introduction

α-Alumina is a dominant ceramic material not only because of its hardness, high temperature strength or chemical inertness, but also because of outstanding dielectrical properties that make it an excellent low- and high- tension insulator. These useful properties have made α-alumina the material of choice for diverse applications ranging from biomedical material (Sedel and Raould, 2007; Wang et al., 2005) to insulators in nuclear fusion reactors (Ibarra and Hodgson, 2004; Mollá et al., 1994).

The knowledge of α-alumina microstructure is essential to understand many of the physical phenomena that take place in this material. In this way, studies about alumina microstructure and its dependency with sintering variables (temperature, dwell time, heating rates, atmospheres, dopants, etc.) have been described in the literature (Lin and De Jongue, 1997; Miranzo et al., 1990). However, practically all this work corresponds to electric furnace sintering. Unfortunately, electrical heating entails a high consume of electric energy and is limited by the maximum sintering temperatures or the heating and cooling rates, depending on the inertia of the elements that integrate the heating system. Furthermore, the conventional sintering techniques usually result in an intensive grain growth of ceramics, producing in many cases materials of coarse grain microstructures. Looking for new sintering systems that overcome these disadvantages, solar furnaces (SFs) offer a possible alternative for fast sintering due to their

* Corresponding author. Tel.: +34 91 346 6578; fax: +34 91 346 6068.
E-mail address: raquel.roman@ciemat.es (R. Román).

0038-092X/$ - see front matter © 2008 Elsevier Ltd. All rights reserved.
doi:10.1016/j.solener.2008.04.002

ability to reach high temperatures in short times and fast heating/cooling rates (several tens of degrees per minute). Moreover, solar radiation is a powerful, ecological and inexhaustible energy source. Due to the large investment costs, solar systems still are seen as an expensive tool but this renewable energy has potential high cost reduction in the medium term. These versatile operation conditions could allow the fabrication of materials with novel microstructures, where the grain growth could be inhibited or the densification rate favoured that will be of interest in some applications. In this way, previous studies have demonstrated the applicability of SFs for sintering process of non-oxide ceramics as Si_3N_4 (Zhilinska et al., 2003), TiC_x (Cruz Fernandes et al., 2002) and WC–Co (Shohoji et al., 2002; Guerra Rosa et al., 2002), or oxide ceramics as alumina (Amaral et al., 2002; Cruz Fernandes et al., 2000), cordierite-based ceramics (Almeida Costa Oliveira et al., 2005) and alumina–magnesia composites (Adylow et al., 1990), being its mechanical properties in many cases comparable to those prepared through conventional sintering processes.

Continuing the research in this particular field, the present work summarizes a detailed sintering study on lab-synthesized alumina powders carried out at the SF of Plataforma Solar de Almería – Spain (PSA-CIEMAT). Several solar sintered tests were performed varying the sintering parameters as temperature, heating rate and atmosphere in order to evaluate their effects on sample microstructures and then to conclude with the optimal solar sintering conditions. The viability of this SF to sinter alumina ceramics is compared with that in an electric furnace.

2. Experimental procedure

2.1. Powder synthesis and processing

The alumina powders tested in this study were synthesized following the homogeneous precipitation with urea route (Hernández et al., 2005; Mishra, 2002). A colloidal suspension was obtained by mixing an aqueous solution containing 0.0075 mol dm^{-3} of $Al(NO_3)_3$ (nonahydrate, Merck, extra pure) as metal supplier and 0.1 mol dm^{-3} of $CO(NH_2)_2$ (Probos) as precipitation agent. The mixed solution was aged at 60 °C for 400 h up to the precipitation of a glassy gel of nanoparticles (300 nm) which was later dehydrated at 100 °C, dried and calcined at 1100 °C to achieve the α-Al_2O_3 phase. The calcined powders were then attrition milled, dried, sieved down to 60 μm and isopressed at 200 MPa to consolidate green compacts. The green bodies were finally presintered at 1200 °C for 4 h to favour their manipulation and then cut into discs of 15 mm in diameter and 2.5 mm in thickness before the solar sintering tests.

2.2. Solar furnace sintering tests

As mentioned above, the solar sintering experiments were carried out in the Solar Furnace of the Plataforma Solar de Almeria (PSA-CIEMAT) in Spain. This solar system (Fig. 1) essentially consists of a continuous solar-tracking flat heliostat, a parabolic concentrator mirror (collector), an attenuator (shutter) and a test zone (test table) located in the concentrator focus centre (Martínez and Rodríguez, 1998). The heliostat reflects horizontal and parallel solar rays on the parabolic collector, which again reflects and concentrates them in its centre (test table area). The flux shutter located between the collector and the heliostat regulates the amount of incident light. Under the centre, the 3D test table permits the position of samples under the focus with the best precision. Its configuration can also be modified depending on samples and carry out experiments. When is 100% open and with a direct solar irradiance of 1000 W m^{-2}, the focus is characterized by an irradiance peak of 3051 kW m^{-2}, a total power of 70 kW and a focal diameter of 26 cm (Rodríguez et al., 2006).

For our sintering tests, the table arrangement consisted of a horizontal alumina cylinder protected by a porous zirconia blanket resulting on a chamber closed with a quartz window (Fig. 2). The chamber is connected to a gas mixture preparing system which permits to work under different controlled atmospheres. Centered in the focus, the presintered samples were placed vertically with respect to the solar layer and exposed to the concentrated direct solar light beam (Fig. 2). Temperature of the system was controlled by two alumina protected thermocouples: a type C (W–Re) at the central test zone and a type B (Pt–Rh) located at the bottom test, in contact with the backside

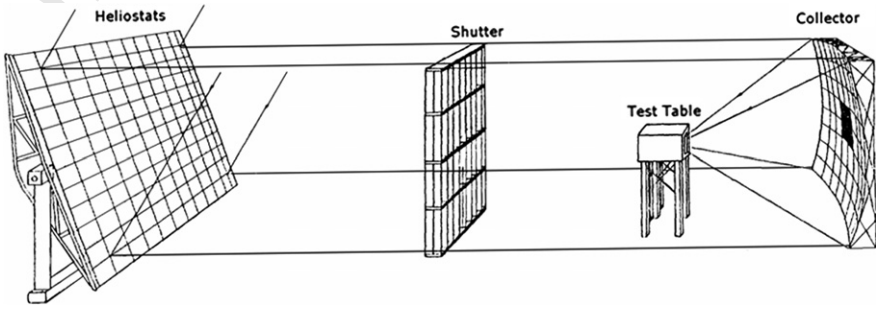

Fig. 1. Functional scheme of the solar furnace (PSA-CIEMAT).

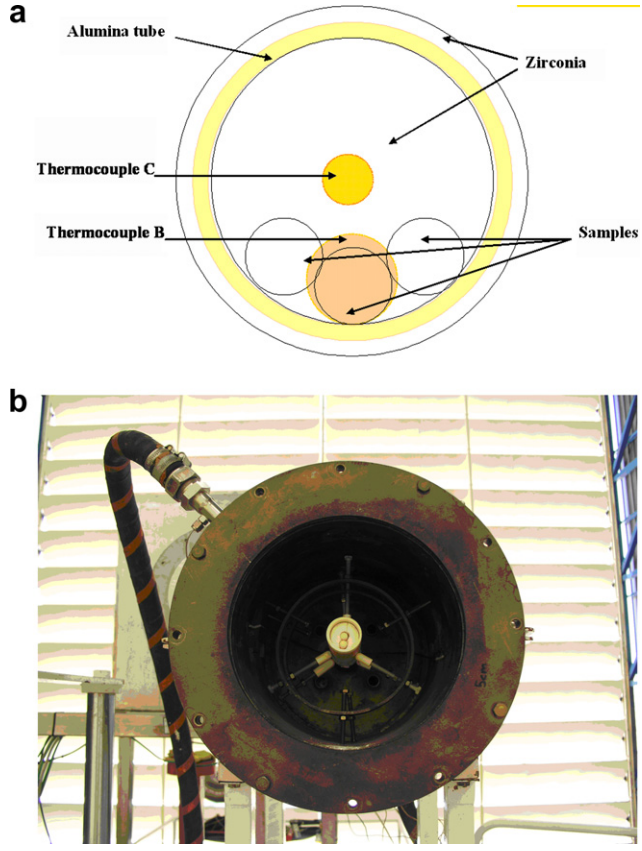

Fig. 2. Scheme of the test table arrangement for the solar furnace experiments and real view of the vacuum chamber with the set-up to the alumina sintering process.

of the sample discs. In addition, the temperature profile was controlled using an infrared equipment consisting of an Avio TVS2000 contactless temperature measurement system and a PC. The IR camera is here used to monitor a profile of the relative temperature distribution along the chamber surface. Absolute temperatures are not measured since the alumina emissivity as a function of temperature was not available.

Taking advantage of the great versatility of this SF, presintered discs were subjected to five sintering tests varying the process parameters (heating rate, temperature and atmosphere) in order to study their influence on the densification rate and on the samples microstructure. For comparison, similar discs were sintered in an electric furnace using conventional sintering conditions. Table 1 summarizes the detailed heating conditions of solar furnace (hereafter labelled as SF experiments) and electric furnace (labelled as EF) sintering tests as well as the main features of the sintered samples.

2.3. Characterization methods

Chemical analysis of calcined, lab-synthesized alumina powders were carried out using a multielemental ICP-OES spectrometer (Thermo Jarrell Ash, mod. IRIS ADVANTAGE).

The particle size of the dried precursor gel and the calcined alumina powders were measured at room temperature by photon correlation spectroscopy (PCS), using a 500 mW Argon laser particle size analyzer (model 4700, Malvern) working with a wavelength of 514 nm.

Bulk densities of the sintered bodies were determined by the Archimedes method (ASTM Standard designation C20-87) with distilled water as the immersion medium. Densities lower than 90% of theoretical were calculated from the experimental weight and volume of samples.

Microstructures of sintered materials were examined using scanning (SEM) and transmission (TEM) electron microscopies. For SEM examination, the samples were sectioned, ground, polished down to 1 μm diamond paste and thermally etched at 25 °C below sintering temperatures during 30 min to reveal the grain boundaries. These etched-polished microstructures were then analyzed using a scanning electron microscope (Hitachi S-2500 at 25 kV). Mean grain size was calculated on SEM micrographs by the linear intercept method (Mendelson, 1969). For exhaustive examination, TEM was conducted, using a TEM-EDX (Philips TECNAI 20 T at 200 kV). TEM sample preparation required sample polishing, dimpling and ion-milling until electron beam transparency.

Additional chemical analysis of sintered samples were carried out by electron probe microanalysis (JEOL Superprobe JXA-8900M) on those specimens prepared to TEM studies in order to determine distributions of elements in matrix particles and along alumina interfaces.

Table 1
Sintering parameters and main features of materials sintered in the solar furnace (SF) of PSA-CIEMAT and in a conventional electric furnace (EF)

TEST	Sintering conditions				Experimental results		
	Heating rate (°C min^{-1})	T (°C)	Dwell time (min)	Atmosphere	D^* (% Dth)	Mean grain size (μm)	Comments
EF1	5	1600	240	Air	89	50	Low densification; irregular grains
SF1	50	1600	60	Air	95	40	Densified matrix; polygonal grains
SF2	100	1600	60	Air	91	30	Slightly restraint of grain growth
SF3	50	1780	60	Air	99	100	High grain growth; external contamination
SF4	50	1600	60	Argon	98	50	Comparable to SF1
SF5	50	1600	60	$95N_2$:$5H_2$	99	100	High grain growth

Presintered sample discs: density: 57% Dth; mean grain size: 2 μm
* Dth (α-Al_2O_3): 3.97 g cm^{-3}

Please cite this article in press as: Román, R. et al., Solar sintering of alumina ceramics: Microstructural development, Sol. Energy (2008), doi:10.1016/j.solener.2008.04.002

3. Results and discussion

3.1. Solar and electric sintering comparison

As a first approach, the feasibility of SFs to consolidate the alumina ceramics was tested by the SF1 experiment, in which the presintered discs were treated under a standard SF operation condition. For comparison of results, similar samples were heated in a conventional furnace using standard sintering conditions (EF1 experiment). The sintering processes and the used parameters are well described in Table 1.

The microstructures obtained after each sintering treatment are shown in Figs. 3 and 5. As can be seen, there are considerable differences between both microstructures depending on the furnace and sintering conditions used during the consolidation process. In this way, samples heated by solar energy (Fig. 3) result in a densified alumina matrix of well defined polygonal grains. The original nanometric particles (300 nm) undergo a homogeneous grain growth during the solar treatment showing a mean grain size value of 20 μm. Moreover, a significant number of spherical shape voids are present in the microstructure, mainly located within the matrix grains. A different sample preparation for SEM observation (Fig. 4a) clearly shows that most of these voids were initially filled with particles, which probably were removed during the polished for conventional SEM examination. A detailed EDX-TEM test (Fig. 4b) also indicates that the filling material is constituted by isolated alumina grains in contact with other nanometric and crystalline particles (nanocrystals) formed by impurities such as C, Si, Ca, Mg and Fe. Fig. 4a shows some crystalline ZrO_2 grains of tetragonal structure filling occasionally the triple points and grain boundaries of the alumina matrix. The chemical analysis (Table 2) show a high impurity content which must be introduced during the extensive powders processing. Since the composition presents a considerable amount of SiO_2 and CaO impurities, the existence of glassy second phase on the alumina microstructure is expected which will influence the material behaviour. Different preparations and observations have led to the conclusion that voids were the consequence of entrapped gases from the residual organic compounds of the starting powders. As it is well known, pores containing big volumes of gas migrate faster during sintering collapsing at the grain boundaries (GBs) and triple points (TPs),

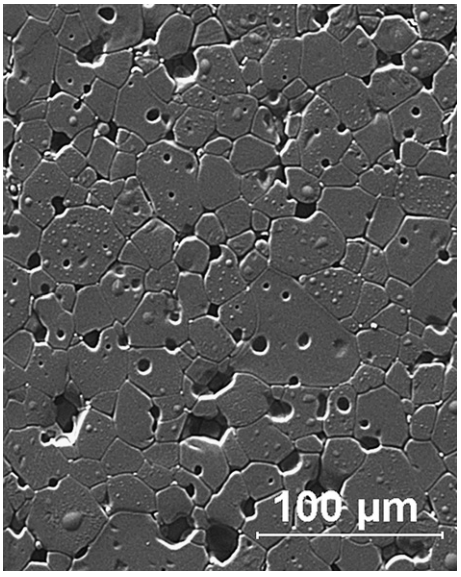

Fig. 3. Microstructure of sample "SF1" sintered in a solar furnace. Sintering conditions: heating rate: 50 °C min^{-1}; temperature: 1600 °C; dwell time: 60 min; atmosphere: air.

Table 2
Main impurities in Al_2O_3 synthesized powders before sintering

	ZrO_2	SiO_2	CaO	MgO	HfO	P_2O_5	Fe_2O_3	Cr_2O_3
Impurities (wt.%)	1.40	0.48	0.13	0.11	0.04	0.04	0.03	0.03

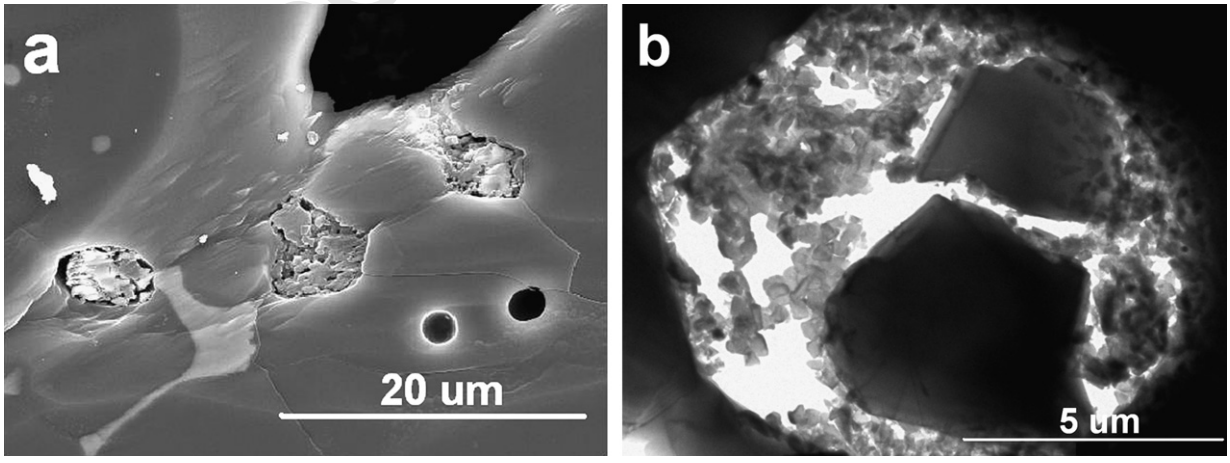

Fig. 4. (a) SEM micrograph of sample "SF1", showing the presence of soft aggregates on the filled voids and a very contrasted second phase of zirconia at grain boundaries; (b) TEM image of a void containing nano and microcrystalline particles of alumina.

Please cite this article in press as: Román, R. et al., Solar sintering of alumina ceramics: Microstructural development, Sol. Energy (2008), doi:10.1016/j.solener.2008.04.002

but the little ones keep entrapped inside matrix grains. The consequence of a very quick consolidation process is that the gas is not allowed to progress to the sample surface, the voids remaining at any depth inside the materials volume. Voids are then shown after samples polishing. The existence of original particles of alumina as soft accumulations inside these big gas-filled pores is due to a lack of diffusion between non-consolidated particles which results in a deficiently sintered material. In addition, impurifying material in concentration above the solubility limit on the alumina solid solution was also diluted in these pores coating the alumina nanoparticles aggregates. Due to the weak bonding with the void walls, these aggregates were easily eliminated during polishing preparation to SEM observations. Very small ones are still decorating some alumina grains, those that could not reach the triple points.

However, when the same composition is sintered by heating in a resistance furnace (Fig. 5), the material densification was not achieved and only a few sintering areas are observed. A considerable pore fraction and irregular grains of about 50 μm of mean grain size showing curvilinear boundaries form the poorly densified microstructure. The majority of voids in EF-sintered samples are located at the grain boundaries with a few isolated pores located within the grains.

Observing the microstructure, the calculated density values using Archimedes method are better pointing out the existence of a close porosity. The frequent but spherical voids observed in SF-samples are in agreement with a calculated density of 95% Dth if a network of isolated voids exists (see Table 1). The high density measured of a sintered body with the observed microstructure is consistent with a network of isolated voids without way out at surface. The remaining closed porosity existing after the quick solar sintering process is revealed after surface polishing. On the other hand, conventional sintering has led to samples with densities of just 89% of the theoretical density (Table 1), a lower density value that can be predicted from the EF-microstructure. It seems evident that the consolidation process was different under the radiation from solar or resistance furnaces, achieving higher densification when solar sintering is applied. Previous works about solar sintering already demonstrated the applicability of these solar systems for production of consolidated ceramic powders with properties comparable to those obtained by conventional sintering (Almeida Costa Oliveira et al., 2005; Guerra Rosa et al., 2002; Cruz Fernandes et al., 2000). The referenced authors sintered ceramic discs by solar radiation and compared the fracture toughness with those sintered in an electric furnace. Their results showed similar density values for solar- and electric-sintered samples as well as comparable microhardness and fracture toughness. Although these authors did not performed microstructural studies, the analogous mechanical behaviour could be indicating a similar grain size for both kinds of samples. In our case, the resultant microstructure of solar sintering samples allows the conclusion that an improvement in material densification and homogeneity of the ceramic grains size has been achieved in comparison to that obtained by electric heating.

3.2. Effect of operation parameters in solar sintering treatments: heating rate and dwell temperature

In order to evaluate the capability of SFs to achieve microstructures of smaller grain sizes, a solar sintered test was performed using a fast heating rate of 100 °C min^{-1} (SF2). The microstructure of the resultant sintered sample is shown in Fig. 6. Comparing the mean grain size with that obtained after heating at 50 °C min^{-1} (SF1), the higher heating rate slightly limits the grain growth. However, con-

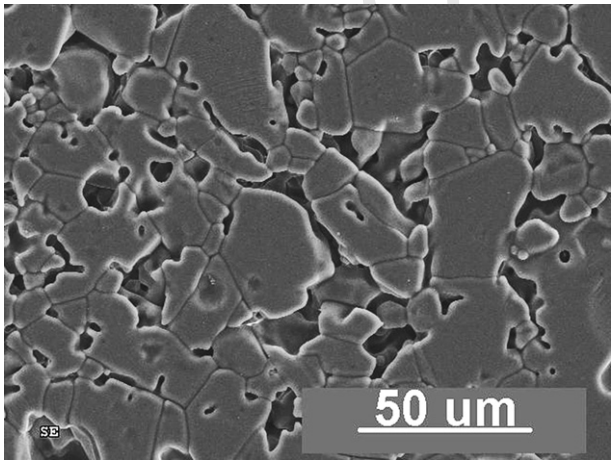

Fig. 5. Microstructure of sample "EF1" sintered in an electric furnace. Sintering conditions: heating rate: 5 °C min^{-1}; temperature: 1600 °C; dwell time: 240 min; atmosphere: air.

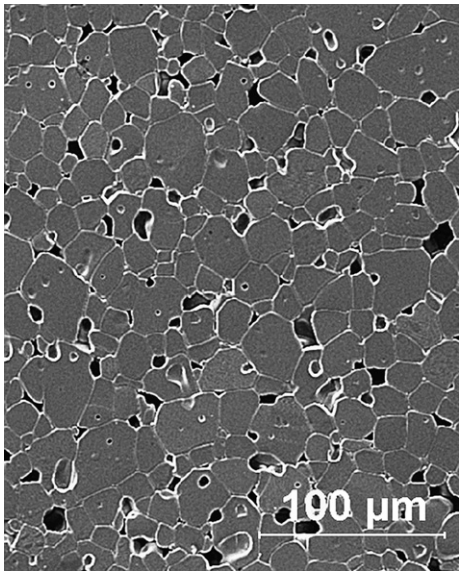

Fig. 6. Microstructure of sample "SF2" sintered in a solar furnace. Sintering conditions: heating rate: 100 °C min^{-1}; temperature: 1600 °C; dwell time: 60 min; atmosphere: air.

sidering 2 μm as the measured matrix mean grain size of presintered discs, observations suggest that faster heating rates do not produce any effective "freezing" of the grain growth. Additionally, the reach of high sintering temperatures at fast heating rates (100 °C min^{-1}) led a big volume of gas get trapped in the bulk microstructure. The result is a higher void volume fraction (probably interconnected) together with lower densities (see Table 1 for the calculated values). Moreover, it must be mentioned that during the 100 °C min^{-1} heating rate, a quick shrinkage of the front surface of samples was obtained. This phenomenon was due to the high temperature so fast achieved in the surface facing the solar radiation in comparison with the face in contact with the zirconia cloth. Although alumina is a good thermal conducting material, the existence of the void network together with the presence of both a glassy SiO_2–CaO and ZrO_2 intergranular phases diminishes the heat conduction, giving rise to a fast densification and considerable shrinkage on the ceramic surface exposed to the solar light.

Taking advantage of the high temperatures that SFs can reach, a sintering test was tried at 1800 °C in order to observe the microstructural differences with respect to that at 1600 °C. During the experiment and above 1650 °C it was observed that sample discs underwent a partial fusion. Once the system was stabilized, a sintering temperature of 1780 °C was achieved (SF3). The partial fusion may be explained in terms of the high content of impurities that might cause a decrease of the alumina melting point. A selected SEM micrograph is shown in Fig. 7. As can be seen, the increase of temperature up to 1780 °C results in a significant enhancement of densification and grain growth. The microstructure is formed by a dense alumina matrix of big equiaxial grains (~100 μm) in which spherical voids are again presented. The same second phases detected in samples sintered at 1600 °C could be observed at this higher temperature, although the zirconia phase content seems to have increased. This qualitative observation was confirmed by the electron probe microanalysis (EPMA) of sintered samples. Figs. 8 and 9 collect the backscattered electron image (a) and the Zr (b), Si (c) and Ca (d) semiquantitave elemental mappings on 1780 and 1600 °C samples, respectively. The grain boundaries of 1780 °C-sample are filled mainly with a rather wide deposit of zirconia (Fig. 8b) together with a less abundant second phase of Si and Ca (Fig. 8c and d). On the other hand, the abundance of the zirconia and the siliceous second phases is not comparable to the 1600 °C-sample microstructure and they are found to be distributed in different matrix regions. In this case, zirconia is located as isolated grains at triple points (Fig. 9b) while Si and Ca impurities are found at grain boundaries (Figs. 9c and d). The 1780 °C-sample morphology is consistent with a composite of alumina, zirconia and a grain boundary glassy phase in accordance to Witek (Witek and Butler, 1986) who ascribed the rounded morphology of the intergranular ZrO_2 as a consequence of the presence of a liquid silicate grain boundary phase during sintering. Svancarek et al. (2004) explained, that the formation of this liquid phase is due to the reaction of silicon and calcium together with some Al_2O_3 and the resultant film is located along the grain boundaries. In other words, the compositional maps are showing a significant increase on the zirconia proportion in that sintered at 1780 °C. It led the authors to the following assumption: the zirconia increase on the higher temperature sintered material suggests that the zirconia refractory cloth wrapping the table test could have diffused into the alumina sample, being diluted and mixed with the initial zirconia phase along the grain boundaries and triple points.

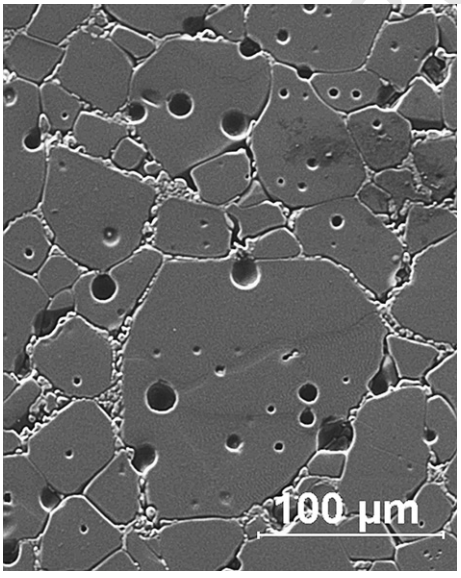

Fig. 7. Microstructure of sample "SF3" sintered in a solar furnace. Sintering conditions: heating rate: 50 °C min^{-1}; temperature: 1780 °C; dwell time: 60 min; atmosphere: air.

At 1780 °C, the sample achieves a density of 99% Dth. Comparing the density results with those at 1600 °C, it seems obvious that densification depends strongly on sintering temperature, increasing the final density from 95% Dth to 99% Dth only by a temperature rise of 180 °C. Nevertheless, this densification increase is also accompanied to a mean grain size enhancement of near the double in respect to that at 1600 °C. It seems to be that alumina dissolution into the silicate amorphous phase has been favoured at 1780 °C giving rise to the abnormal grain growth of some matrix grains. The liquid phase mechanism of alumina sintering seems to be promoted by increasing dwell temperature rather than sintering rate. Then it must be pointed out the important advantage of solar furnaces offering sintered bodies of moderate grain size microstructures in those ceramic materials with high content of impurities.

3.3. Effect of the sintering atmosphere

Finally, tests using atmospheres of argon (SF4) and a 95:5 mixture of N_2:H_2 (SF5) were carried out and their results compared to those obtained in air (SF2). Scanning

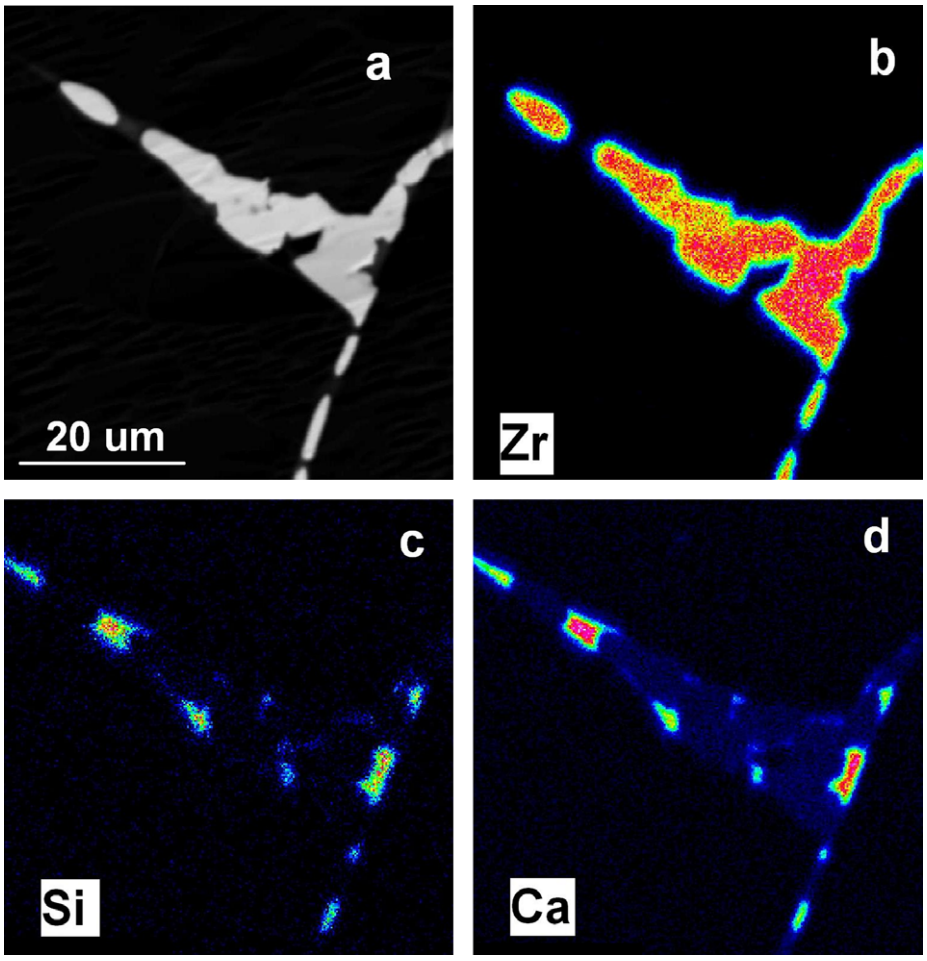

Fig. 8. Microstructure of the Al_2O_3 sample sintered at 1780 °C. (a) Backscattered electron image of grain boundary and the (b) Zr, (c) Si and (d) Ca elemental compositional mappings of the material filling the grain boundaries.

electron micrographs of the three materials (Figs. 3, 10 and 11) revealed some significant differences in microstructure depending on the tested atmosphere.

In this way, the effect of using Ar gas on densification, grain growth and grain morphology is similar to that of air. The microstructure of Ar-samples was also formed by a dense matrix of polygonal and homogenous alumina grains of about 50 μm and several inter and intragranular spherical pores. The ZrO_2 second phase is also detected at triple junctions. A sensible difference between the mean grain sizes distinguishes SF2 and SF4 samples. The density seems to be a little favoured when sintering in an inert atmosphere, since a density value of 98% Dth is calculated.

When samples were sintered in a $95N_2$:$5H_2$ gas mixture, an effective matrix sintering is deduced from a microstructure of big equiaxed alumina grains with a mean grain size of 100 μm (Fig. 11). An important fraction of intragranular pores is visible together with a residual intergranular porosity. The densification is enhanced using this atmosphere, obtaining a density value of 99% Dth, while only a 95% Dth is reached in air. The experimental density results fully correspond to the density variation obtained when gases of different molecular weight are entrapped in close voids. In other words, considering sintered aluminas of similar volume fraction of close porosity, an Ar gas of higher molecular weight compared to air or a $95N_2$:$5H_2$ mixture filling the inside of closed voids would result in a ceramic body of higher density, which would give rise to a comparable density.

The microstructural differences between the materials would be mainly explained due to gas solubility in alumina during the final stage of sintering. At this stage the pores pinch off and become isolated and therefore the environmental gas is trapped inside pores. Then a way of porosity elimination is the gas diffusion through the matrix grains. According to this, Coble (1962) found that MgO-doped Al_2O_3 could be sintered up to theoretical density in O_2 and H_2, but not in air, N_2, He or Ar because of their different solubilities. The solubility is related to gas molecules size, so small molecules like H_2 or O_2 can easily diffuse during sintering, increasing the total density. Big gas molecules as those in air, N_2, He or Ar have a limited solubility in Al_2O_3 so they keep trapped in the matrix network, limiting the densification. Our results are in agreement to this discussion, showing air and Ar microstructures with a considerable densification, but also abundant spherical voids

Please cite this article in press as: Román, R. et al., Solar sintering of alumina ceramics: Microstructural development, Sol. Energy (2008), doi:10.1016/j.solener.2008.04.002

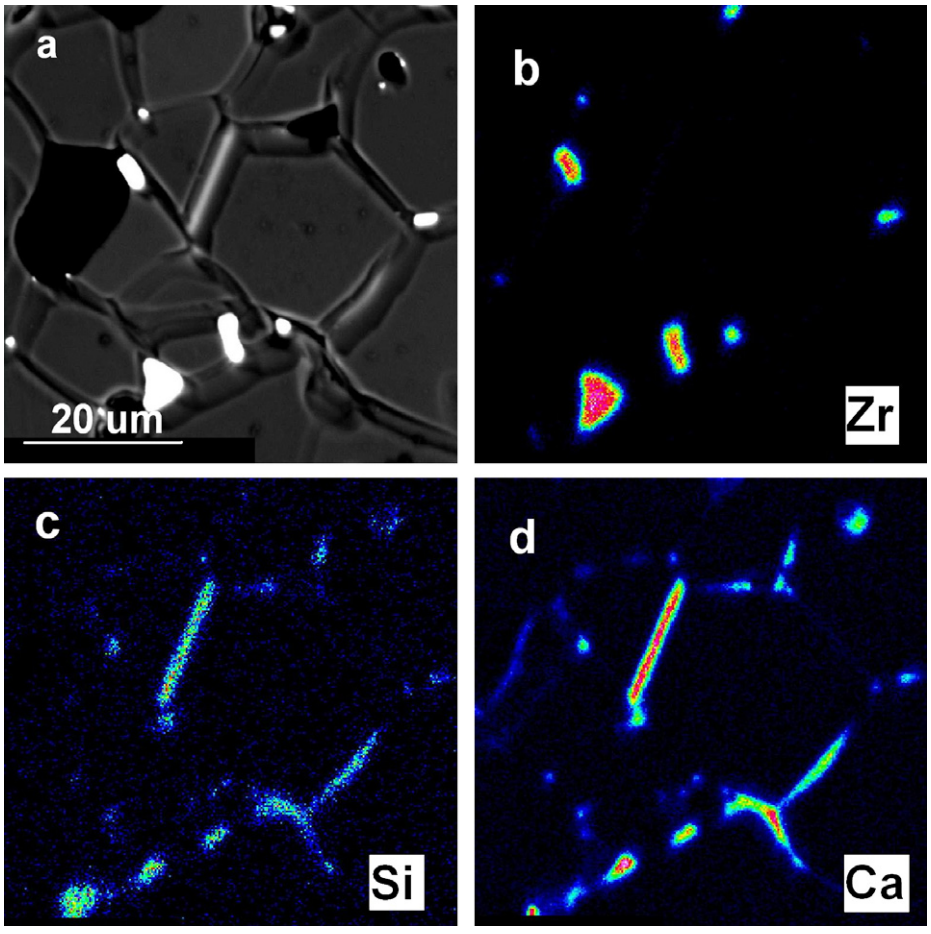

Fig. 9. Microstructure of the Al_2O_3 sintered at 1600 °C. (a) Backscattered electron image of grain boundary and the (b) Zr, (c) Si and (d) Ca elemental compositional mappings of the material filling the grain boundaries.

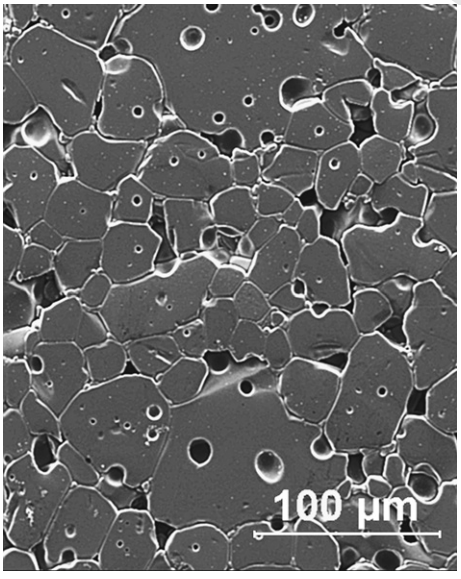

Fig. 10. Microstructure of sample "SF4" sintered in a solar furnace. Sintering conditions: heating rate: 50 °C min^{-1}; temperature: 1600 °C; dwell time: 60 min; atmosphere: Ar.

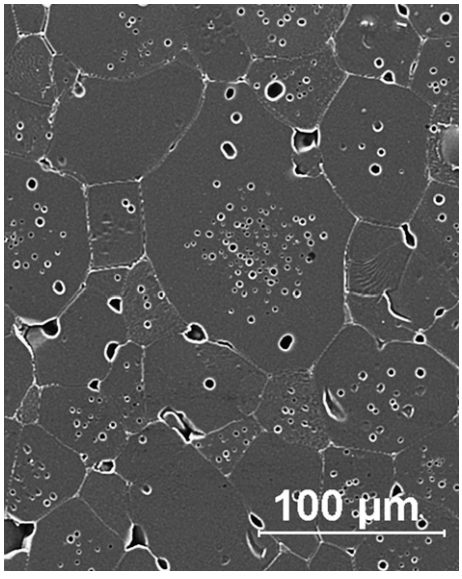

Fig. 11. Microstructure of sample "SF5" sintered in a solar furnace. Sintering conditions: heating rate: 50 °C min^{-1}; temperature: 1600 °C; dwell time: 60 min; atmosphere: $95N_2$:$5H_2$.

caused by the gas trapped in the matrix. Considering that air is composed mainly by nitrogen and oxygen (78% N_2; 21% O_2) and that the reducing atmosphere includes 95% N_2 and only a 5% H_2, it is difficult to understand only in

Please cite this article in press as: Román, R. et al., Solar sintering of alumina ceramics: Microstructural development, Sol. Energy (2008), doi:10.1016/j.solener.2008.04.002

terms of hydrogen diffusivity why it favours the densification and grain growth of the sintered material. Probably the reducing character of the H_2 is also playing a significant role, creating a number of oxygen vacancies in the alumina grains enhancing the diffusion of species and therefore improving sintering. Then, the high diffusivity and the reducing character of hydrogen would produce the efficient pore elimination during sintering as well as the improvement of mass transportation through grain boundaries. It can be observed in the microstructure as an effective grain growth in which very small pores still remain inside grains. In agreement with this, it must be pointed out that a grey colour was observed on SF-ceramic bodies after reducing atmosphere sintering in respect to the presintered discs. The colour change maybe then supporting the idea of oxygen vacancies formation during sintering.

4. Concluding remarks

Synthesized α-alumina powders were subjected to different solar sintering treatments by modifying the heating rate, the sintering temperature and the furnace atmosphere. The obtained microstructures of a complex alumina matrix are in agreement with the presence of some impurities (mainly SiO_2, CaO, ZrO_2 and MgO) distributed at grain boundaries, triple points and matrix voids. The resultant inter and intragranular voids are formed due to the accumulation of residual organic compounds of the starting powders, causing lower after-sintering calculated densities than those expected from alumina compacted discs.

The capability of the solar device to sinter ceramics was tested by comparing samples subjected to conventional sintering at an electric furnace. The results show significant differences between solar and electric sintering microstructures. In particular, solar sintering favours the densification of these alumina samples difficult to consolidate by conventional sintering without applied pressure. The simultaneous high heating rates and short sintering times during solar treatments are convenient parameters to restrain grain growth.

It was observed that grain growth is promoted by increasing sintering temperature rather than heating rate. The increase of sintering temperature above 1780 °C results in a significant enhancement of densification (99% Dth), but a partial fusion of samples occurred. At this temperature, the zirconia content located as a second phase at grain boundaries and triple points has been increased which might be the consequence of contamination during material softening from the zirconia cloth that protects the furnace table. These results indicate that the use of temperatures up to 1600 °C in solar systems seems not to be appropriated to achieve microstructures of small grains.

A comparison of microstructures after solar sintering under air, Ar and $95N_2{:}5H_2$ atmospheres was performed. The higher diffusivity and the reducting character of H_2 could be the explanation of the more efficient pore elimination as well as the improvement of mass transportation that gives rise to the biggest grains but also achieves the highest densification of the alumina matrix.

Near future experiments are being designed to increase temperature and heating rate using alumina powders without residual organic matter and with very low impurities level. Then it would be desirable to achieve well densified and small grained final microstructures

5. Uncited references

Cho et al. (2003), Hart and LeRoy (1990)). Q1

Acknowledgments

The authors would like to thank to G. de Velasco y F.J. Galindo (Solar Furnace of PSA-CIEMAT) for their valuable help in these experiments, as well as to A. del Rio (SEM-CIEMAT), J. González (TEM-URJC) and The Electronic Microscopy Center "Luis Bru" (EPMA and SEM-UCM) for the microstructural analysis. This work has been cofinanced by CICYT through Project FTN2003-03855 and forms part of the European Fusion Technology Programme.

References

Adylow, G.T., Bibershtein, B.E., Voronov, G.V., Urazaeva, É.M., 1990. Alumina–magnesia spinel based ceramic produced in a solar furnace. Refract. Ind. Ceram. 31 (9–10), 499–502.

Almeida Costa Oliveira, F., Shohoji, N., Cruz Fernandes, J., Guerra Rosa, L., 2005. Solar sintering of cordierite-based ceramics at low temperatures. Sol. Energ. 78, 351–361.

Amaral, P.M., Anjinho, C., Cruz Fernandes, J., Guerra Rosa, L., Shohoji, N., 2002. Fracture toughness of alumina ceramic disks sintered in a solar furnace and subsequently cooled with relatively fast rate (50 K/min). In: Proceedings of 8th Portuguese Conference on Fracture, Sociedade Portuguesa de Materiais, Vila Real, Portugal, pp. 395–399.

ASTM Standard designation C20-87.

Cho, S.-J., Lee, Y.-C., Lee, H.-L., Sim, S.-M., Yanagisawa, M., 2003. Chemical inhomogeneity in commercial alumina powders and its effect on abnormal grain growth during sintering. J. Eur. Ceram. Soc. 23, 2281–2288.

Coble, R.L., 1962. Sintering alumina: effect of atmospheres. J. Am. Ceram. Soc. 45 (3), 123–127.

Cruz Fernandes, J., Amaral, P.M., Guerra Rosa, L., Shohoji, N., 2000. Weibull statistical analysis of flexure breaking performance for alumina ceramic discs sintered by solar radiation heating. Ceram. Int. 26, 203–206.

Cruz Fernandes, J., Anjinho, C., Amaral, P.M., Guerra Rosa, L., Rodríguez, J., Martínez, D., Almeida Costa Oliveira, F., Shohoji, N., 2002. Characterisation of solar-synthesized TiC_x ($x = 0$, 50, 0.626, 0.75, 0.85, 0.90 and 1.0) by X-ray diffraction, density and Vickers microhardness. Mater. Chem. Phys. 77, 711–718.

Guerra Rosa, L., Amaral, P.M., Anjinho, C., Cruz Fernandes, J., Shohoji, N., 2002. Fracture toughness of solar-sintered WC with Co additive. Ceram. Int. 28, 345–348.

Hart, I., LeRoy, D., 1990. Alumina Chemicals: Science and Technology Handbook. Wiley-American Ceramic Society.

Hernández, T., Bautista, C., Martín, P., 2005. Synthesis and thermal evolution of Mn-doped alumina nanoparticles by homogeneous precipitation with urea. Mater. Chem. Phys. 92, 366–372.

Ibarra, A., Hodgson, E.R., 2004. The ITER project: the role of insulators. Nucl. Instrum. Meth. Phys. Res. Sect. B 218, 29–35.

Lin, F.J.T., De Jongue, L.C., 1997. Microstructure refinement of sintered alumina by a two-step sintering technique. J. Am. Ceram. Soc. 80 (9), 2269–2277.

Martínez, D., Rodríguez, J., 1998. Surface treatment by concentrated solar energy: the solar furnace at the "Plataforma Solar de Almería". In: Surface Modification Technologies XI, proceedings of the 11th International Conference on Surface Modification Technologies, Paris, France, pp. 441–447.

Mendelson, M.I., 1969. Average grain size in polycrystalline ceramics. J. Am. Ceram. Soc. 52 (8), 443–446.

Miranzo, P., Tabernero, L., Moya, J.S., Jurado, J.R., 1990. Effect of sintering atmosphere on the densification and electrical properties of alumina. J. Am. Ceram. Soc. 73 (7), 2119–2121.

Mishra, P., 2002. Low-temperature synthesis of α-alumina from aluminium salt and urea. Mater. Lett. 55, 425–429.

Mollá, J., Heidinger, R., Ibarra, A., 1994. Alumina ceramics for heating systems. J. Nucl. Mater. 212–215, 1029–1034.

Rodríguez, J., Cañadas, I., Fernández, J., Monterreal, R., Ballestrín, J., Téllez, F., Yebra, L., 2006. The PSA solar furnace, a test facility ready to characterize high-concentration solar devices from solar thermal applications to PV cells. In: Proceedings of 13th International Symposium on Concentrated Solar Power and Chemical Energy Technologies, ISBN: 84-7834-519-1.

Sedel, L., Raould, A., 2007. Engineering aspect of alumina on alumina hip prosthesis. Proc. Ins. Mech. Eng., Part H: J. Eng. Med. 221 (1), 21–27.

Shohoji, N., Guerra Rosa, L., Cruz Fernandes, J., 2002. Extending horizon of materials processing with solar furnace. Paper presented at the IHP-Users Workshop 2002.

Svancarek, P., Galusek, D., Calvert, C., Loughran, F., Brown, A., Brydson, R., Riley, F., 2004. A comparison of the microstructure and mechanical properties of two liquid phase sintered aluminas containing different molar ratios of calcia–silica sintering additives. J. Eur. Ceram. Soc. 24, 3453–3463.

Wang, Z., Xue, D., Chen, X., Lü, B., Ratajczak, H., 2005. Mechanical and biomedical properties of hydroxyapatite-based gradient coating on α-Al_2O_3 ceramic substrate. J. Non-Cryst. Solids 351 (19–20), 1675–1681.

Witek, S.R., Butler, E.P., 1986. Zirconia particle coarsening and the effects of zirconia additions on the mechanical properties of certain commercial aluminas. J. Am. Ceram. Soc. 69 (7), 523–529.

Zhilinska, N., Zalite, I., Rodríguez, J., Martínez, D., Cañadas, I., 2003. Sintering of nanodisperse powders on the basis of silicon nitride in a solar furnace. In: Euro PM 2003 Conference Proceedings, Valencia, Spain, vol. 3. pp. 423–428.

Please cite this article in press as: Román, R. et al., Solar sintering of alumina ceramics: Microstructural development, Sol. Energy (2008), doi:10.1016/j.solener.2008.04.002